Alexandria Engineering Journal (2022) xxx, xxx–xxx

HOSTED BY

ELSEVIER

Alexandria University

Alexandria Engineering Journal

www.elsevier.com/locate/aej
www.sciencedirect.com

All-textile inspired-folded dipole antennas for on/off-body communications medical applications

Farah R. Kareem [a,b,*], **Mohamed El Atrash** [b], **Ahmed A. Ibrahim** [a], **Mahmoud A. Abdalla** [c]

[a] *Communication and Electronics Department, Faculty of Engineering, Minia University, Minia, Egypt, Al Minyā 61512, Egypt*
[b] *Electrical Communication and Electronic Systems Engineering Department, October University for Modern Sciences and Arts, Giza 12563, Egypt*
[c] *Electronic Engineering Department, Military Technical College, Cairo 11787, Egypt*

Received 15 February 2021; revised 6 September 2021; accepted 10 February 2022

KEYWORDS

Artificial magnetic conductor (AMC);
Covid-19;
Folded dipole antenna;
ISM band;
Textile materials wearable flexible antenna

Abstract Two textile-based printed inspired Folded Dipole Antennas (FDAs) are presented in this paper for health monitoring of Covid-19 infected patients. The first antenna has an overall size of 80 mm × 20 mm and is mounted on the human's chest, while the second one is backed by a 2 × 4 textile Artificial Magnetic Conductor (AMC) array structure and is mounted on a surgical mask that covers the human's mouth. The first antenna is designed to work at center frequency, bandwidth, and gain of 2.45 GHz, 116.6 MHz and −2.45 dB, respectively. The second antenna works at 2.4 GHz with bandwidth of 76.6 MHz and gain of 2.71 dB. The SAR results equal 0.524 W/Kg and 0.255 W/Kg at 1 g and 10 g, respectively, for the first antenna and 0.0174 W/Kg and 0.0091 W/Kg, respectively, for the second one. The previous specifications of the two antennas enable them to be utilized in wearable applications and Wi-Fi services.

1. Introduction

Wearable devices have emerged tremendously and are considered a necessity to suit various wearable applications; such as, tracking, navigation, military, sports, and health monitoring. Much of the conducted researches in health monitoring have focused on improving the environment communication link [1,2]. In such systems, the antenna plays an essential role in successful communication for far-field telemetry [3]. Wearable biomedical antennas should hold certain characteristics; for instance, small profile, light weight, flexibility, mechanical influences (bending, crumpling and compression), suitable radiation pattern, and unwanted absorption of radiation by the human body [4–6].

Wearable antennas are designed based on a variety of different fabrication materials to attain flexibility and display robustness against bending cases. Examples include: (1) using ultra-thin and highly flexible polyimides as substrate materials [7–10]. Also, Velcro material has been used for the substrate [11]. (2) Using polydimethylsiloxane (PDMS) [12–14]. (3) Using knitted copper for the metallic patch and ground layers

* Corresponding author.
E-mail address: fkareem@msa.edu.eg (F.R. Kareem).
Peer review under responsibility of Faculty of Engineering, Alexandria University.

https://doi.org/10.1016/j.aej.2022.02.026

[15]. (4) flexible conductive sheet VeilShield [14] and ShieldIt conducting [5]. (5) Silverpan 250 yarns [16]. (6) Conductive inks [17]. Flexible textile embroidered antennas are, usually, counted as good choices for human body wearable services because of their low cost, small losses and simplicity to be integrated into garments [18,19]. Thanks to the large thickness of textile material, the antenna bandwidth is widened so it can cover different frequency bands and can be utilized for different applications [20]. In [21] indigo jeans was incorporated for the substrate material, whereas embroidered textiles were utilized in [19,22].

The electromagnetic interference between the wearable antennas and the nearby human body affects two aspects: (1) the antenna performance; such as, deformation of the radiation patterns, reduction in the antenna efficiency, and detuning of the resonant frequency. (2) Potential health threats to the body. Specific Absorption Rate (SAR) is a parameter which indicates whether or not the antenna is safe for the human body. SAR is calculated in terms of the electric field generated by the antenna (E) using (1), where σ and ρ are the human tissue conductivity and mass density, respectively. To ensure conformance to the FCC's standards for Radio-Frequency (RF) fields close to human bodies, the SAR value should not exceed their standard values limits. There are two standard limits; (a) The American standard, permitted by FCC, has the threshold of 1.6 W/kg averaged over 1 g of tissue as a maximum value. The EU standard, permitted by IEC, has the threshold limit of 2 W/kg averaged over 10 g of tissue.

$$\mathrm{SAR} = \frac{\sigma |\mathrm{E}|^2}{\rho} \tag{1}$$

The lower the SAR value is, the better the antenna can be realized for wearable applications, taking into consideration the other performance parameters. Therefore, many methods for minimizing the SAR were proposed in the literature: (1) increasing the space between the human body and the antennas [23]. (2) Changing the antenna feeding point [24]. (3) Employing metamaterials, (4) Utilizing a ferrite sheet [25]. (5) Including electromagnetic band-gap structures [26]. (6) Utilizing a graphene-type absorbing material [27] between the antenna and human body. (7) Using a reflector element along with the main radiator [28]. (8) Using cavity-backed antenna [29]. (9) Adding an RF shield at the front side of device for the reduction of unnecessary radiations [30]. (10) Using highly directive antennas by placing Split Ring Resonators array between the antenna and human head. (11) Adding AMC surfaces [1,6,31,32]. Using artificial magnetic conductors in wearable applications yields low profile antennas [33] in additional to improving the bandwidth, efficiency, gain and increasing the front–to-back ratio [28,34–36]. Several AMCs operating at 2.45 GHz have been presented in [37]. In [38], Defected Ground Structure (DGS) and Electromagnetic Band Gap (EBG) were used for isolation and to widen the bandwidth.

Examples of successful wearable antennas include half wavelength circular loop antenna [39], and the inverted-F antenna for wireless communications in body area network [40]. Probe-fed textile patch antennas were presented in [36] and aperture coupled methods are introduces in [41]. A compact wearable antenna has been designed using the fractal approach for 2.45 GHz applications [42]. A combination of loop and dipole textile antennas into Yagi-like structure is presented in [43]. An ultra-compact triangular patch antenna was proposed in [44]. A Substrate Integrated Waveguide (SIW)-based antenna was suggested in [45]. A ring-shaped geometry for high optical transparency, flexibility, comprises a simple and planar structure is investigated in [14].

The Folded Dipole Antennas (FDAs) are characterized with wideband impedance characteristics [46,47]. FDA has an omnidirectional radiation pattern when fed with an unbalanced transmission line [48,49], which is required for several wireless comminution applications [47]. In [50], a planer single substrate Huygens dipole antenna was discussed. A T-shaped folded dipole antenna was designed using copper tape in addition to polyester film and was integrated with a two-element EBG in [51]. In [52], a design comprising of printed folded dipole with a ground plane or EBG substrate was proposed. In [53], a folded dipole antenna backed by a 2 × 2 AMC array was introduced, which displayed a heart-shaped-like omni-radiation pattern. In [54], a compact printed folded dipole antenna was presented. In [55], a folded slot antenna, over a 3 × 3 AMC was discussed.

And in [47], a modified planar folded dipole, with coupled feeding structure to obtain three resonant modes was investigated.

Nowadays, the world is suffering from undetectable diseases; hence, new and smart techniques should be thought of to discover them. At the moment, all the world suffers from the huge infection spread of Covid-19 virus. In this paper, two textile-based wearable inspired FDAs, mounted on different human-body parts, are proposed. The first antenna is designed to be on the human's chest for monitoring the heart rate and respiratory rate of the patient unceasingly, while the second one is backed by a 2 × 4 AMC array structure and is placed on the surgical mask covering the patient's mouth to detect the viral disease (flu/influenza) by analyzing the patient's breath. The chest-mounted antenna works at ISM 2.45 GHz, whereas the mouth-mounted antenna works at 2.4 GHz for communicating the patient's vital signs via the Wi-Fi wireless communication standard. Since, the chest-mounted antenna communicates its vital signs to the mouth-mounted integrated design, then the chest-mounted antenna displays an omni-directional radiation pattern. This type of radiation pattern is preferable for the on-body communication link. The integrated design has a uni-directional radiation pattern for transmitting the data wirelessly to a physician, situated at the hospital, for diagnosing the vital signs and deciding whether or not the patient needs assistance. This type of radiation pat-

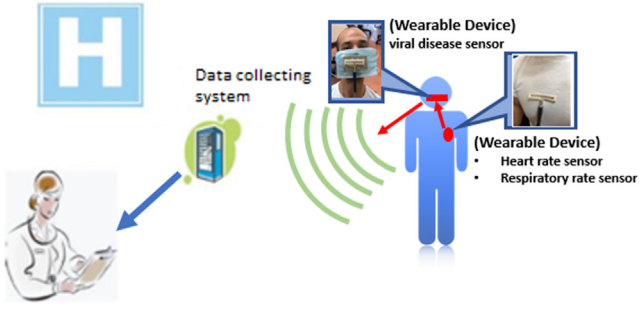

Fig. 1 The proposed antenna system.

tern is preferable for the off-body communication link. The antenna proposed system is shown in Fig. 1.

2. Chest-mounted inspired FDA structre and performance

Introduced in this section is the layout of the inspired FDA, which is realized using textile materials. It is evaluated close to the human body's chest for monitoring the heart and respiratory rates. Evaluation is conducted using the Computer Simulation Technology full-wave simulator tool.

2.1. The proposed antenna structure

The 2D perspective view of the first proposed antenna is shown in Fig. 2 (a). The radiator is an inspired half-wavelength printed FDA with oversize of 8 cm × 2 cm. The Co-Planar Waveguide (CPW) feeding approach is used for excitation. To maintain flexibility and integrate with the clothes, ShieldIt Super with conductivity and thickness of 1.18×10^5 S/m and 0.17 mm is used as conductive material.

Furthermore, the dielectric textile Felt is a porous material that is used for the substrate with 1.5 mm thickness, 1.2 dielectric constant and 0.044 loss tangent, respectively. The conductive textile ShieldIt Super possesses a hot melt adhesive back, which makes it easy to iron it to the dielectric felt substrate. Fabrication was implemented using manual cutting tools, where the finished prototype is portrayed in Fig. 2 (b). Table 1 displays the final dimensions of the proposed antenna.

2.2. The proposed antenna performance

Prior evaluating the antenna within the vicinity of the human chest, it was evaluated in free space where it achieved resonance at the desired frequency of 2.45 GHz. Fig. 3 shows the inspired FDA current distribution at 2.45 GHz. Gain radiation pattern measurements was conducted using the StarLab Antenna Measurement – MVG in the near-field, as displayed in Fig. 4.

The simulated normalized gain radiation pattern is benchmarked against the measured one, in polar forms in the principal planes, at 2.45 GHz, as illustrated in Fig. 5. Inspecting Fig. 5 (a) and Fig. 5 (b), the antenna has bi-directional pattern and omni-directional pattern in the E-plane (∅ = 0°) and H-plane (∅ = 90°), respectively. Both sets of results confirm the fact that the antenna exhibits an omni-directional radiation pattern type. The small disagreements between the simulated and measured results can be claimed because of the manual fabrication and the transformation from the near field to far field. The simulated realized gain and total efficiency at the broad-side direction are −3.39 dB and 23.1%, respectively. From the measurement perspective, they are −3.12 dB and 27.4%, respectively. The simulated co-polarized and cross-polarized patterns in the H-plane are illustrated in Fig. 6, where it is highly evident that the proposed antenna is linearly polarized.

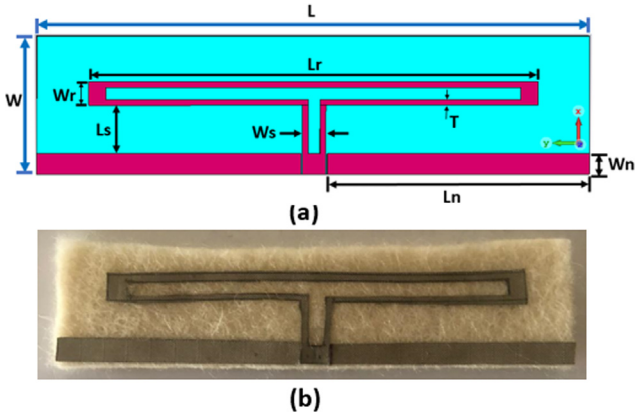

Fig. 2 The 2D layout and geometry of (a) Printed inspired FDA; (b) Fabricated textile prototype resonating at 2.45 GHz.

Subsequently, the antenna is tested at distance of 10 mm away from the Hugo human model chest to make up for the patient's outfit, which is realized using Fleece, as depicted in Fig. 7. Fig. 8 shows the measured and simulated results of S_{11}, which also shows the measuring setup of the fabricated antenna in the inset. It is shown that the reflection coefficient of the chest-mounted inspired FDA operates at 2.45 GHz with a −10 dB fractional bandwidth of 4.8 % and exhibits good impedance matching of −16 dB for the simulation scenario. Whereas for the tested scenario, the −10 dB fractional bandwidth is 8.33% with a good impedance matching of −18 dB.

The relatively wide bandwidth is due to the fact that antenna is realized using thick (1.5 mm) textile substrate (felt), which possesses a low dielectric constant of 1.2. Furthermore, the measured fractional bandwidth is slightly wider than the simulated one better matching.

These differences can be explained by the uncertainty concerning the textile substrate properties and the mechanical inexactness caused by the manual fabrication procedure with simple manual tools. The fabrication was done by cutting the materials manually, using a manual cutter, which makes a little difference in the dimensions. This difference in dimensions led to a difference between measured and simulation results. The most important point is that the antenna performance still fulfills the requirements for the required frequency band.

The chest- mounted FDA displays the 3D conventional omni-directional gain radiation pattern with a gain of −2.45 dB, as shown in Fig. 9. Since, the chest-mounted antenna (first inspired FDA) communicates its vital signs to the second antenna, then it is preferable that the chest-mounted antenna displays an omni-directional radiation pattern to suit the on-body communication link. Moreover, the exhibited low gain is attributed to the antenna small footprint. The SAR results at 2.45 GHz equal 0.524 W/Kg and 0.255 W/Kg averaged over 1 g and 10 g, respectively, based on the IEEE C95.1–2005 with the input power of 0.1 W, as shown in Fig. 10 (a) and Fig. 10 (b). The attained levels abide to the US and EU standards. Thus, the antenna is safe for operation near the human body.

3. Mouth-mounted integrated design structre and performance

To operate at close distances to the human body and attain uni-directional radiation pattern type, a 2 × 4 all-textile AMC array structure is used at the back of the inspired FDA. The inspired FDA longest dimension is slightly modified, so that it resonates at 2.4 GHz; however, it maintains

Table 1 The first fda dimensions (mm).

Par.	L	W	Lr	Wr	Ls	Ws	T	Ln	Wn
Dim.	80	20	65	3.4	7.85	3.4	0.85	38.1	3

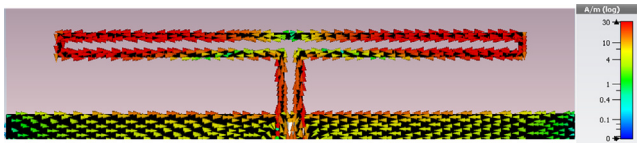

Fig. 3 The inspired FDA current distribution at 2.45 GHz in free space.

Fig. 4 The setup for measuring the standalone inspired FDA radiation pattern.

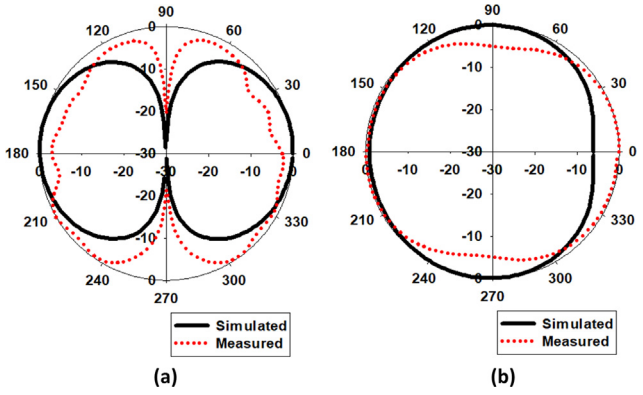

Fig. 5 The normalized simulated and measured gain radiation patterns for 2.45 GHz for: (a) at φ = 0° (X-Z plane); (b) at φ = 90° (Y-Z plane).

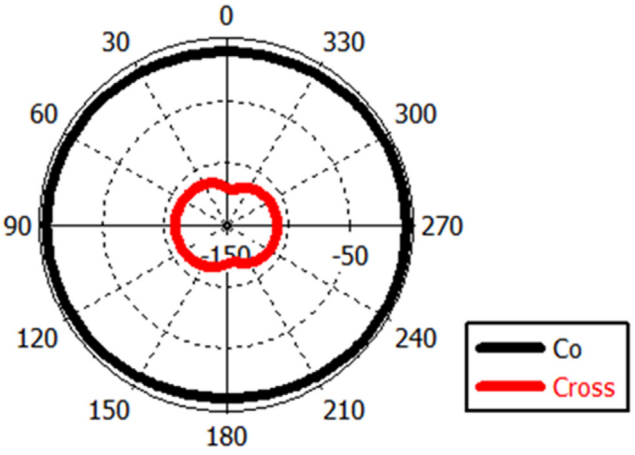

Fig. 6 Simulated co- and cross-polarized H-plane radiation patterns of inspired FDA at 2.45 GHz.

its overall footprint of 80 mm × 20 mm. The antenna is designed at this specific frequency to communicate over the Wi-Fi wireless communication standard.

3.1. The AMC design and characterization

The proposed 2 × 4 all-textile AMC array structure, which possesses a size of 100 mm × 50 mm, with a periodicity of 25 mm, is demonstrated in Fig. 11 (a). The number of column elements is higher than the row elements in order to suit mounting it on the surgical mask. Displayed in Fig. 11 (b) is the unit-cell, which is based on loading the patch with a cross-shaped slot, where its longest dimension is 20 mm. In this way, the overall design is minimized, since the loading of the slot lengthens the current path that increase the inductance, which leads to a reduction in size, as indicated in equation (2) [56]. Following equation (2), the unit-cell dimensions were attained to achieve operation at 2.4 GHz [56]. The unit-cell footprint is 24.8 mm × 24.8 mm.

$$f = \frac{1}{2\pi\sqrt{LC}} \tag{2}$$

To ensure that the proposed design possesses AMC features, it has to hold Perfect Magnetic Conductor (PMC) characteristics. The unit-cell was studied by incorporating periodic boundary conditions at its sides and was illuminated with a

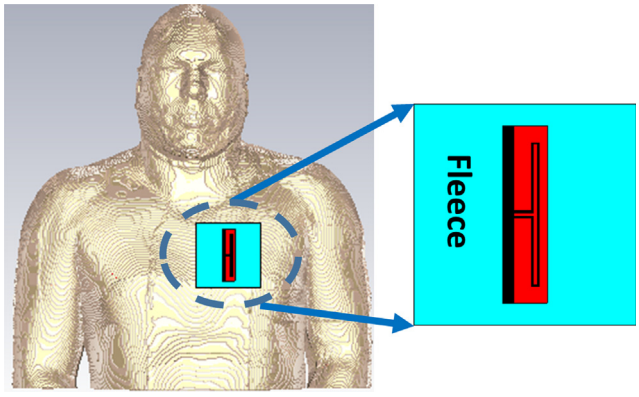

Fig. 7 The setup for evaluating the inspired FDA against the Hugo human body model.

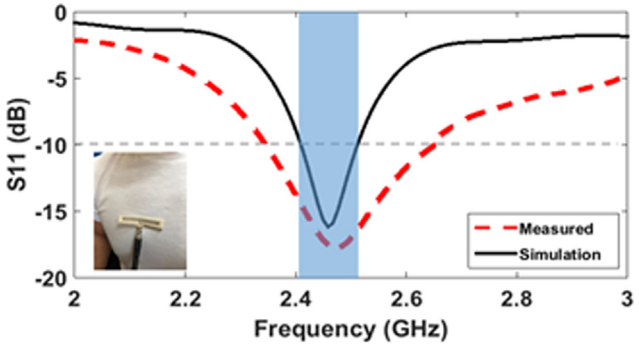

Fig. 8 The simulated and measured S_{11} of the inspired FDA with an inset of the chest loading scenario.

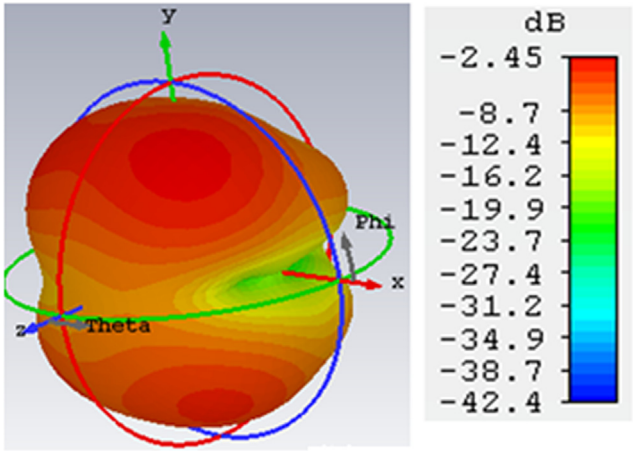

Fig. 9 The inspired FDA 3D gain radiation pattern against the Hugo human body model at 2.45 GHz.

waveguide port that is distanced by half-wavelength from the top patch. Portrayed in Fig. 12 (a) and Fig. 12 (b) are the unit-cell characteristics. It is seen from Fig. 12 (a) that, the zero-reflection phase is accomplished at the designed 2.4 GHz, with bandwidth (calculated from a −90° to +90°) extending from 1.44 to 2.66 GHz. The second feature is to exhibit high impedance at the operating frequency, which is

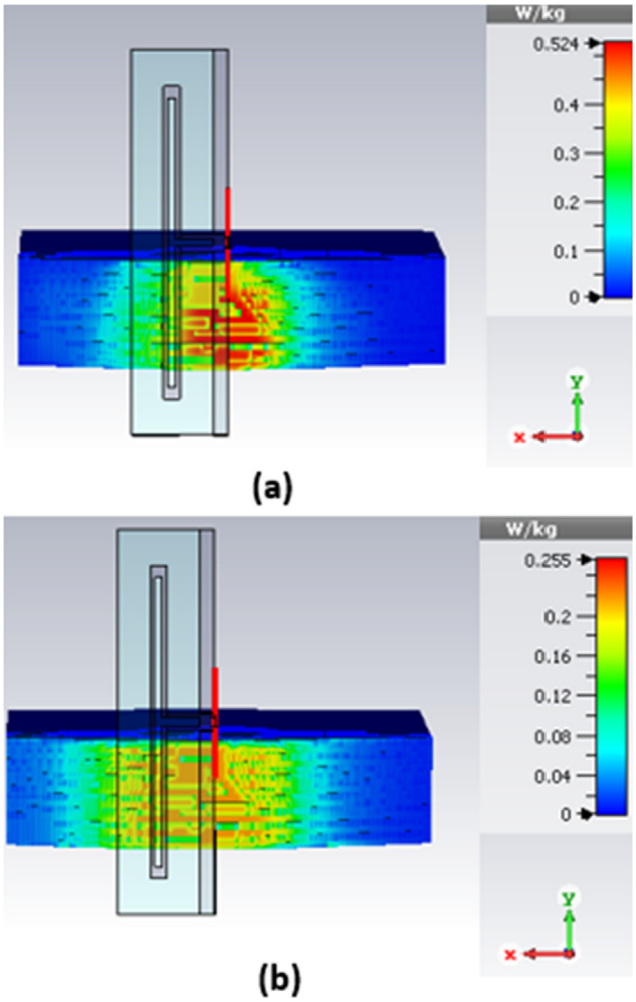

Fig. 10 The inspired FDA SAR levels at 2.45 GHz averaged over: (a) 1 g; (b) 10 g.

shown in the same Fig. 12 (a), where the unit-cell exhibits an impedance of 7.1 kΩ at 2.4 GHz. The third property is to exhibit a band-gap at 2.4 GHz, which is depicted in Fig. 12 (b) by inspecting the dispersion diagram.

3.2. The inspired FDA-backed AMC array structure

Accordingly, the AMC array structure is realized using the same textile materials, as the inspired FDA, which were ShieldIt for the conductive fabric and felt for the dielectric one. The separate structures' layouts are displayed in Fig. 13 (a) and Fig. 13 (b), while the integrated design strapped to the surgical mask setup is demonstrated in Fig. 13 (c). Fig. 14 shows the simulated S_{11} results of the inspired FDA in free space with and without the AMC array structure. It is seen that two results have the same trend which confirms the proposed design. The normalized simulated radiation patterns, with and without AMC, in free space at 2.4 GHz, at both $\varphi = 0°$ and $\varphi = 90°$ planes, are shown in Fig. 15. It is noticed that the both antenna cases have bi-directional pattern and omni-directional pattern in E–plane and H-plane, respectively.

Distanced by 2 mm from the human mouth, the integrated design was evaluated, as illustrated in Fig. 16 and the inset of

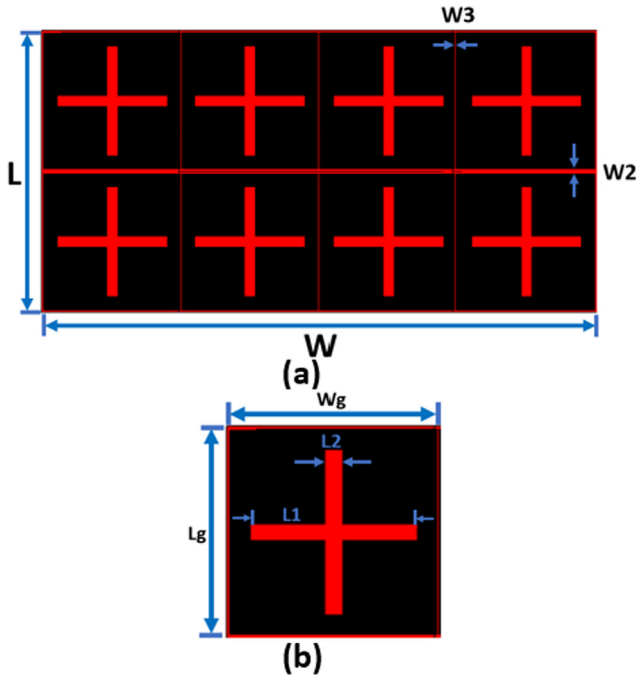

Fig. 11 2D Layout of: (a) AMC array structure (W = 100 mm, L = 50 mm, W2 = 0.9 mm and W3 = 0.2 mm); (b) AMC unit cell (Wg = 24.8 mm, Lg = 24.8 mm, L1 = 20 mm and L2 = 2 mm).

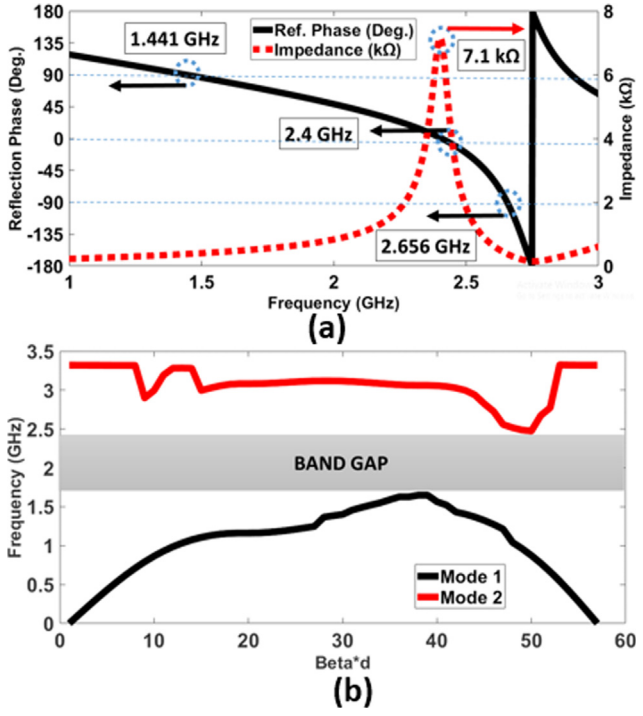

Fig. 12 The simulated features of AMC unit-cell: (a) Reflection phase and input impedance; (b) Dispersion diagram, illustrating band-gap region.

Fig. 17 (a). The different antenna parameters, including the SAR levels, are evaluated in this scenario. The simulated and measured S_{11} is demonstrated in Fig. 17 (a). From the simula-

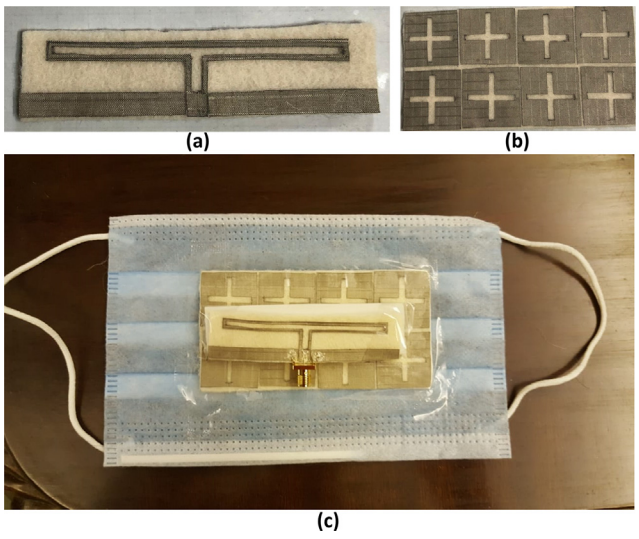

Fig. 13 The 2.4 GHz fabricated: (a) Inspired FDA; (b) AMC array structure; (c) Integrated antenna design mounted and strapped to the surgical mask.

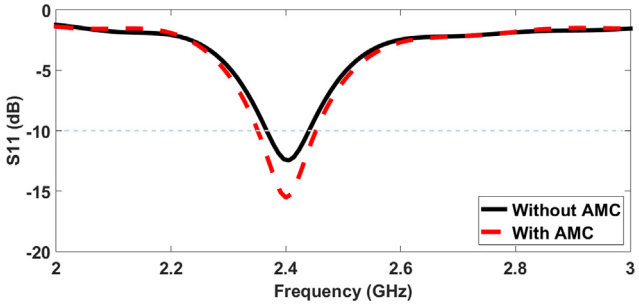

Fig. 14 The simulated S_{11} of the inspired FDA in free space with and without AMC.

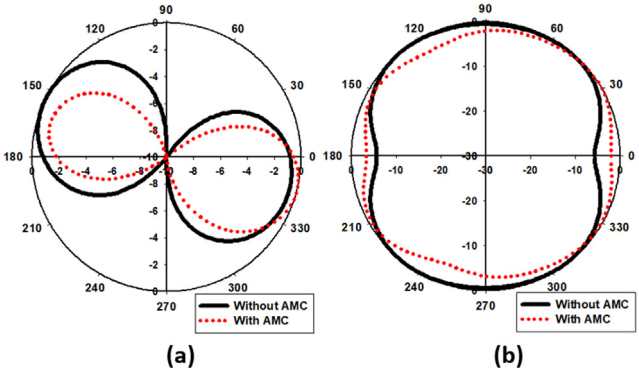

Fig. 15 The normalized simulated gain radiation patterns with and without including AMC array structure in free space for 2.4 GHz for: (a) at φ = 0; (b) at φ = 90.

tion perspective, the proposed united design operates at 2.4 GHz with S_{11} of −12.5 dB and fractional bandwidth (-10 dB) of 3.2%. On the other hand, the tested results exhibit a better matching of −20 dB and fractional bandwidth of 8.33%. The difference between simulated and tested results;

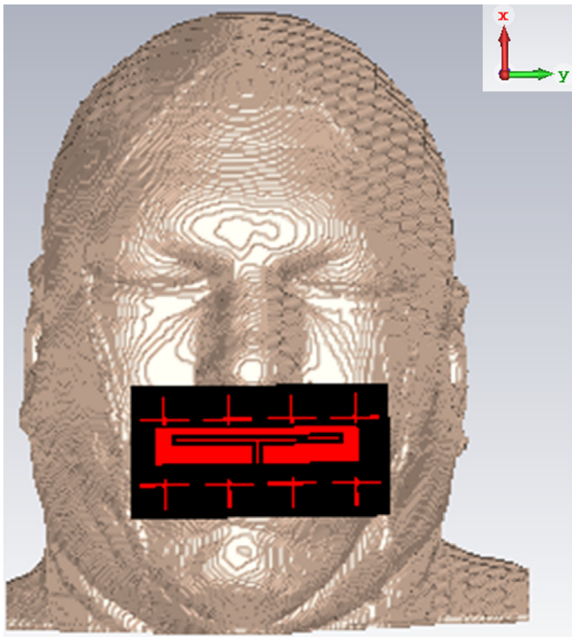

Fig. 16 The setup for evaluating the printed FDA, including AMC array structure, against the Hugo human face model face.

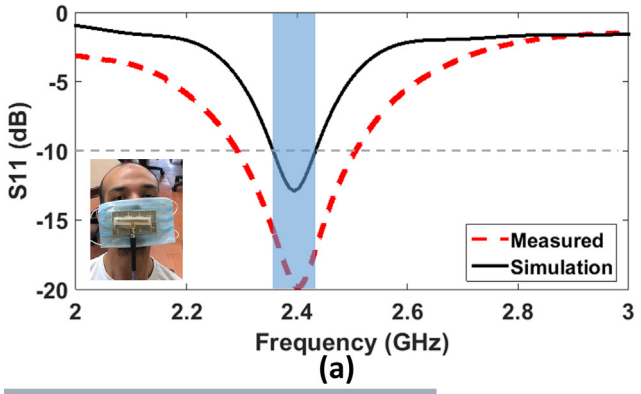

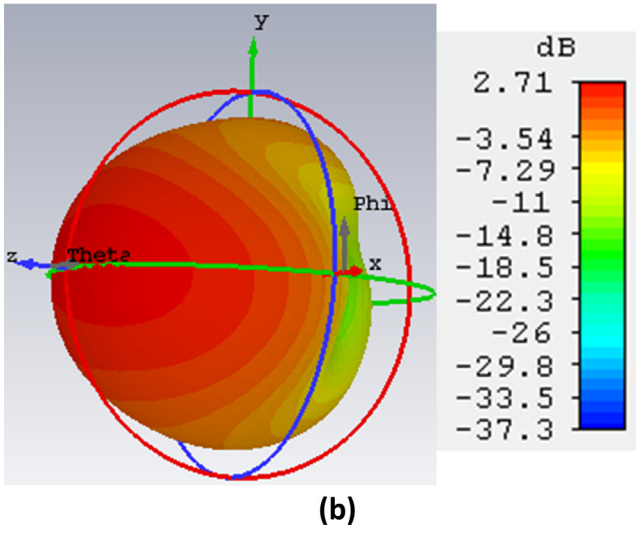

Fig. 17 The integrated design when loaded by the surgical mask and subject's mouth: (a) Simulated against measured reflection coefficients; (b) 3D gain at 2.4 GHz.

this can be explained by the previous reasons discussed in Section 2.2

The 3D gain radiation pattern is displayed in Fig. 17 (b) with a gain of 2.71 dB, where the gain of the simulated antenna on the mouth without AMC was 1.96 dB; that explains the benefits of AMC in the gain enhancement of the proposed antenna.

The united design draws directional radiation pattern type because of the backing reflector. This kind is desirable for the off-body communication link, as the integrated design objective is to send the patient's symptoms, located at home, to the doctor, located at the hospital. The aim is to detect the viral disease (flu/influenza) by analyzing the patient's breath.

While the SAR values of FDA without AMC at 2.4 GHz are 1.57 W/Kg and 0.688 W/Kg, average over 1 g and 10 g of tissues, respectively as presented in Fig. 18 (a) and Fig. 18 (b). These SAR values are below the permissible limit but still, we need to decrease it to be this proposed system safer to safe levels. Finally, the united design SAR levels in such a condition, at 2.4 GHz, are 0.0174 W/Kg and 0.0091 W/Kg, averaged

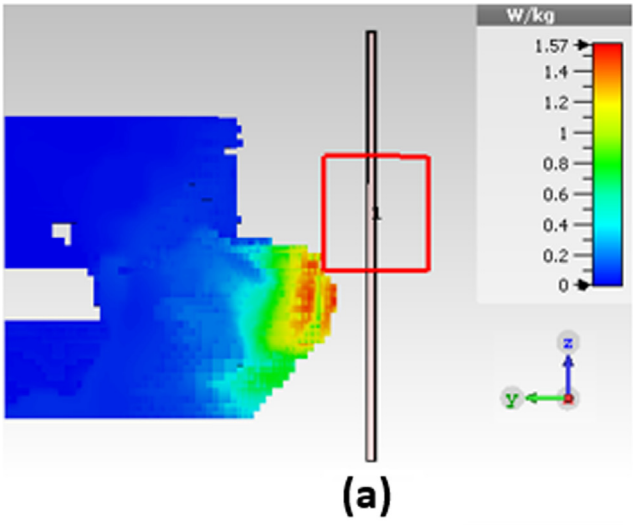

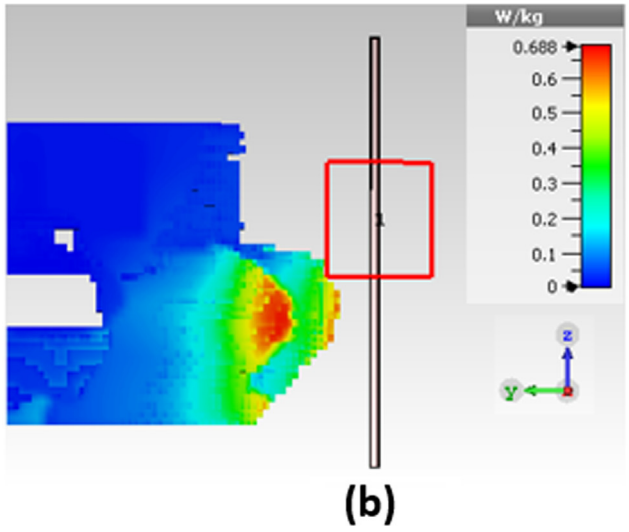

Fig. 18 The FDA (Without AMC) SAR levels at: (a) 1 g; (b) 10 g.

over 1 g and 10 g of tissues, respectively as illustrated in Fig. 19 (a) and Fig. 19 (b), correspondingly. Moreover, it can be seen that from the side view of Fig. 19 that the AMC is distanced from the inspired FDA to avoid interactions between the SMA connector and the AMC top patch.

The IEEE C95.1–2005 standard with the input power of 0.1 W is used to evaluate the SAR values. Based on the disseminated results, the integrated design functions suitably within the vicinity of the human mouth and are un-harmful, as per the very low SAR outcomes. The obtained SAR results abide to the US and EU standards.

4. Coupling effect

In this section, the mutual coupling effect between both antennas is highlighted. Mutual coupling leads to extra power loss in case the antennas are placed close to one another [48]. Since two antennas are mounted on the human body; hence, it is considered a vital parameter to consider. Displayed in Fig. 20, the setup for measuring the coupling level, which indicates the amount of energy transmitted from the shoulder-mounted antenna (inspired-FDA) to the mouth-mounted one (integrated antenna). It is worth noting that that transmission is from the inspired FDA antenna, since it holds an omnidirectional radiation pattern desired for on-body communications, for communicating its data to the integrated design one.

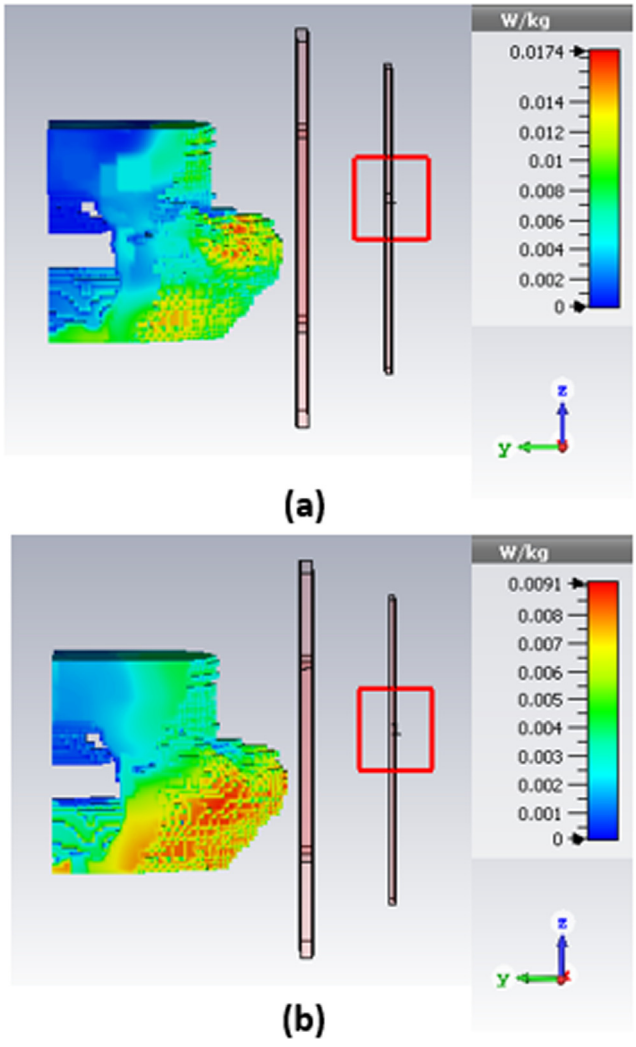

Fig. 19 The FDA (including AMC array structure) SAR levels at: (a) 1 g; (b) 10 g.

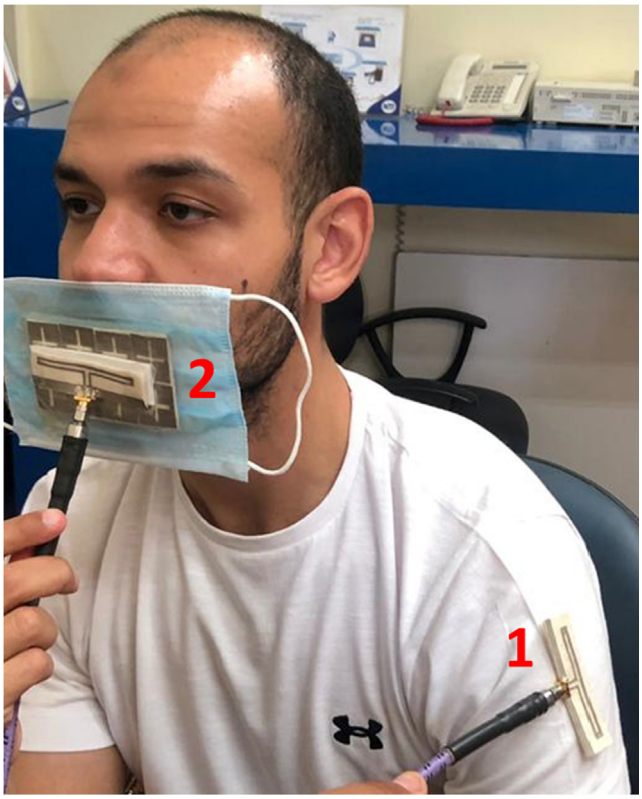

Fig. 20 The setup for measuring the coupling level between both wearable antennas.

The tested coupling level is demonstrated in Fig. 21, where the transmission coefficient (S_{21}) is below −45 dB over the entire spectrum. This very low outcome is due to a number of reasons. First is the fact that both antennas do not share a common ground level. Secondly, the antennas are positioned on different human body parts that are spaced apart. The separation between both antennas is important in the reduction of the coupling level, since it is well-known that the coupling

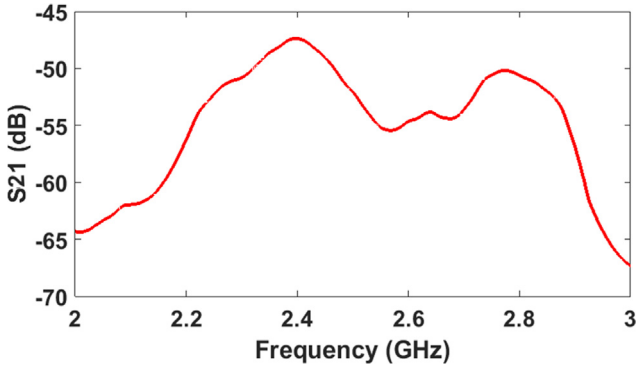

Fig. 21 The measured coupling level between both wearable antennas.

Table 2 Comparison between different folded dipole antenna designs.

Antenna Design	Materials	Frequency (GHz)	Gain (dB)	Antenna Electrical Size	Reflector Type/Physical Size (mm^2)	Max. SAR (W/kg)
[44]	A Metal Composite Embroidery Yarn and Polyester woven substrate	0.0925	N/A	0.473 λ0 × 0.00306 λ0	N/A	N/A
		0.102		0.474 λ0 × 0.0034 λ0		
		0.106		0.477 λ0 × 0.0035 λ0		
		0.113		0.486 λ0 × 0.0037 λ0		
		0.118		0.477 λ0 × 0.0039 λ0		
[47]	copper sheet/F4B substrates	1.57	1.27	0.3 λ0 × 0.15 λ0	N/A	N/A
[48]	Copper tape/Polyester film	2.4	6.26	0.384 λ0 × 0.304 λ0	EBG/74 × 37	0.09
[49]	Copper adhesive foil	0.406	7	0.406 λ0 × 0.027 λ0	metallic foil / 150 × 350 × 90	N/A
[51]	Copper/Rogers substrate	5	N/A	0.3083 λ0 × 0.016 λ0	AMC/65 × 65	N/A
[52]	N/A	2.45	N/A	0.0735 λ0 × 0.236 λ0	N/A	N/A
[55]	Rogers (RO3003)	2.4	2.6 dB	0.472 λ0 × 0.248 λ0	AMC/76 × 88	0.8
[58]	RO4003	2.4	3 dB <	1.02 λ0 × 0.82 λ0	AMC/125 × 100	N/A
[32]	latex substrate	2.4	1.81	0.576 λ0 × 0.576 λ0	Double Layer AMC/ 50 × 50	0.714
[60]	RT/Duroid 5880	2.4/5.2	5 dBic	0.4 λ0 × 0.4 λ0	AMC/72 × 72	N/A
[59]	ShieldIt Super/Felt	2.4/5	4 dB <	0.358 λ0 × 0.372 λ0	AMC/100 × 100	0.0464
Proposed design	ShieldIt Super/Felt	2.4 GHz	2.71	0.64 λ0 × 0.16 λ0	AMC/100 × 51	0.0091

magnitude between two nearby antennas is proportional to the position of one antenna relative to the other [56].

Finally, the comparison between our proposed united design and the recent FDA-related united designs in the literature are tabulated in Table 2. The proposed design is based on textile materials for ease of integration with garments; hence, it is highly flexible. Also, it exhibits low SAR levels in comparison with [57].

Despite that the proposed AMC array is larger than [48] and [51], it is smaller than [49,58,59]. Furthermore, it is all-textile with high flexibility and durability. Also, it had a very low SAR value when compared with other wearable antenna which makes it safe for wearing long and continuous period. In addition to the gain, it is suitable for medical application. In spite of the size may not be considered small enough but it can still be accommodating the targeted application of mounting it on the surgical mask.

5. Conclusion

Introduced in this paper are two printed CPW-fed and textile-based inspired FDAs, mounted on the chest and mouth, for health monitoring applications. Both hold compact size, light weight, high degree of flexibility, and robustness against human body loading. The antenna installed on the chest is a half-wavelength inspired FDA, which radiates at 2.45 GHz, with an area of 0.653 $\lambda_0 \times 0.163\ \lambda_0$, for monitoring the respiratory rate as an indication for Covid-19 detection. It has gain of −2.45 dB with omni-directional radiation pattern features. The proposed inspired FDA, which is installed on the surgical mask prior to being mounted on the mouth, is backed by an AMC array structure of 2 × 4 unit cells. The integrated structure resonates at 2.4 GHz, with an entire area of $0.8\ \lambda_0 \times 0.408\ \lambda_0$, for monitoring the user's health conditions and serving the Wi-Fi wireless service. It has gain of 2.71 dB with uni-directional radiation pattern characteristics. The SAR levels of the two proposed antennas are lower than US and EU limits. Based on the underlined outcomes, the proposed antennas might be utilized for wearable medical applications, specifically monitoring Covid-19 symptoms, ISM applications, and Wi-Fi applications.

Declaration of Competing Interest

The authors declare that they have no known competing financial interests or personal relationships that could have appeared to influence the work reported in this paper.

References

[1] L. Yao, E. Li, J. Yan, Z. Shan, X. Ruan, Z. Shen, Y. Ren, J. Yang, Miniaturization and electromagnetic reliability of wearable textile antennas, Electron. 10 (9) (2021) 994, https://doi.org/10.3390/electronics10090994.

[2] H. Kunsei, K.S. Bialkowski, M.S. Alam, A.M. Abbosh, Improved Communications in Underground Mines Using Reconfigurable Antennas, IEEE Trans. Antennas Propag. 66 (12) (2018) 7505–7510.

[3] P.S. Hall, Y. Hao, Antennas and Propagation for Body-Centric Wireless Networks, Artech House, 2006.
[4] Amor Smida, Amjad Iqbal, Abdullah J. Alazemi, M.I. Waly, R. Ghayoula, S. Kim, Wideband Wearable antenna for Biomedical Telemetry applications, IEEE Access 8 (2020) 15687–15694.
[5] S.N. Mahmood, A.J. Ishak, T. Saeidi, A.C. Soh, A. Jalal, M.A. Imran, Q.H. Abbasi, Full ground ultra-wideband wearable textile antenna for breast cancer and wireless body area network applications, Micromachines 12 (3) (2021) 322, https://doi.org/10.3390/mi12030322.
[6] M. El Atrash, M.A. Abdalla, H.M. Elhennawy, A Compact Highly Efficient Π-Section CRLH Antenna Loaded with Textile AMC for Wireless Body Area Network Applications, IEEE Trans. Antennas Propag. 69 (2) (2021) 648–657.
[7] M. El Atrash, M.A. Abdalla, H.M. Elhennawy, Gain enhancement of a compact thin flexible reflector-based asymmetric meander line antenna with low SAR, IET Microwaves, Antennas Propag. 13 (6) (2019) 827–832.
[8] M. El Atrash, M.A. Abdalla, H.M. Elhennawy, A Wearable Dual-Band Low Profile High Gain Low SAR Antenna AMC-Backed for WBAN Applications, IEEE Trans. Antennas Propag. 67 (10) (2019) 6378–6388.
[9] S.R. Zahran, M.A. Abdalla, A. Gaafar, A flexible wide band single fed slot antenna with circular polarizing rotated elliptical ground and impulse response, Int. J. Microw. Wirel. Technol. 11 (9) (2019) 872–884.
[10] S.R. Zahran, M.A. Abdalla, A. Gaafar, New thin wide-band bracelet-like antenna with low SAR for on-arm WBAN applications, IET Microwaves, Antennas Propag. 13 (8) (2019) 1219–1225.
[11] B. Sanz-Izquierdo, F. Huang, J.C. Batchelor, Small size wearable button antenna, Eur. Sp. Agency, (Special Publ. ESA SP) 626 SP (December 2014) (2006) 2–6.
[12] C.P. Lin, C.H. Chang, Y.T. Cheng, C.F. Jou, Development of a flexible SU-8/PDMS-based antenna, IEEE Antennas Wirel. Propag. Lett. 10 (2011) 1108–1111.
[13] Z.H. Jiang, Z. Cui, T. Yue, Y. Zhu, D.H. Werner, Compact, Highly Efficient, and Fully Flexible Circularly Polarized Antenna Enabled by Silver Nanowires for Wireless Body-Area Networks, IEEE Trans. Biomed. Circuits Syst. 11 (4) (2017) 920–932.
[14] A.S.M. Sayem et al, Optically Transparent Flexible Robust Circularly Polarized Antenna for UHF RFID Tags, IEEE Antennas Wirel. Propag. Lett. 19 (12) (2020) 2334–2338.
[15] H.H. Pekka Salonen*, A Novel Fabric WLAN Antenna For Wearable Applications, Tilmpeie Univ. ofTechnology I In∼titufc Electron., 2019, pp. 698–700.
[16] Y. Liu, M. Yu, L. Xu, Y. Li, T.T. Ye, Characterizations and Optimization Techniques of Embroidered RFID Antenna for Wearable Applications, IEEE J. Radio Freq. Identif. 4 (1) (2020) 38–45.
[17] U. Hasni, M.E. Piper, J. Lundquist, E. Topsakal, Screen-Printed Fabric Antennas for Wearable Applications, IEEE Open J. Antennas Propag. 2 (March) (2021) 591–598.
[18] C.X. Mao, Y. Zhou, Y. Wu, H. Soewardiman, D.H. Werner, J. S. Jur, Low-Profile Strip-Loaded Textile Antenna with Enhanced Bandwidth and Isolation for Full-Duplex Wearable Applications, IEEE Trans. Antennas Propag. 68 (9) (2020) 6527–6537.
[19] C.X. Mao, D. Vital, D.H. Werner, Y. Wu, S. Bhardwaj, Dual-Polarized Embroidered Textile Armband Antenna Array with Omnidirectional Radiation for On-/Off-Body Wearable Applications, IEEE Trans. Antennas Propag. 68 (4) (2020) 2575–2584.
[20] D.L. Paul, H. Giddens, M.G. Paterson, G.S. Hilton, J.P. McGeehan, Impact of body and clothing on a wearable textile dual band antenna at digital television and wireless communications bands, IEEE Trans. Antennas Propag. 61 (4) (2013) 2188–2194.
[21] S. Sankaralingam, B. Gupta, A circular disk microstrip WLAN antenna for wearable applications, in: Proc. INDICON 2009 - An IEEE India Counc. Conf., 2009, pp. 3–6.
[22] Z. Wang, L.Z. Lee, D. Psychoudakis, J.L. Volakis, Embroidered multiband body-worn antenna for GSM/PCS/WLAN communications, IEEE Trans. Antennas Propag. 62 (6) (2014) 3321–3329.
[23] R.Y.S. Tay, Q. Balzano, N. Küster, Dipole configurations with strongly improved radiation efficiency for hand-held transceivers, IEEE Trans. Antennas Propag. 46 (6) (1998) 798–806.
[24] J. Kim, M. Abdel-Mageed, C. Pelletti, R. Mittra, L. Li, SAR reduction of multi-band antenna by using Partially Reflective Surfaces, in: IEEE Antennas Propag. Soc. AP-S Int. Symp., vol. 2015-Octob, 2015, pp. 370–371.
[25] J.N. Hwang, F.C. Chen, Reduction of the peak SAR in the human head with metamaterials, IEEE Trans. Antennas Propag. 54 (12) (2006) 3763–3770.
[26] K. Han, M. Swaminathan, R. Pulugurtha, H. Sharma, R. Tummala, S. Yang, V. Nair, Magneto-Dielectric Nanocomposite for Antenna Miniaturization and SAR Reduction, IEEE Antennas Wirel Propag. Lett. 15 (2016) 72–75.
[27] M.B. Manapati, R.S. Kshetrimayum, SAR reduction in human head from mobile phone radiation using single negative metamaterials, J. Electromagn. Waves Appl. 23 (10) (2009) 1385–1395.
[28] K. Chen, Z. Yang, Y. Feng, B. Zhu, J. Zhao, T. Jiang, Improving microwave antenna gain and bandwidth with phase compensation metasurface, AIP Adv. 5 (6) (2015) 067152, https://doi.org/10.1063/1.4923195.
[29] H. Memarzadeh-Tehran, R. Abhari, M. Niayesh, A cavity-backed antenna loaded with complimentary split ring resonators, AEU - Int. J. Electron. Commun. 70 (7) (2016) 928–935.
[30] J.M. George, A Review on SAR Reduction Methods Used For Mobile Application, IOSR J. Electron. Commun. Eng. Ver. II 10 (5) (2015) 2278–2834.
[31] Q. Liu, H. Liu, W. He, S. He, A low-profile dual-band dual-polarized antenna with an AMC reflector for 5G communications, IEEE Access 8 (2020) 24072–24080.
[32] K. Agarwal, Y.-X. Guo, B. Salam, Wearable AMC Backed Near-Endfire Antenna for On-Body Communications on Latex Substrate, IEEE Trans. Components, Packag. Manuf. Technol. 6 (3) (2016) 346–358.
[33] Y.F. Cao, X.Y. Zhang, T. Mo, Low-Profile Conical-Pattern Slot Antenna with Wideband Performance Using Artificial Magnetic Conductors, IEEE Trans. Antennas Propag. 66 (5) (2018) 2210–2218.
[34] V.A. Almeida Filho, A.L.P.S. Campos, Performance optimization of microstrip antenna array using frequency selective surfaces, J. Microwaves, Optoelectron. Electromagn. Appl. 13 (1) (2014) 31–46.
[35] M.I. Ibrahim, S.I. El-Henawy, A.M.E. Safwat, "60 GHz Artificial Magnetic Conductor loaded dipole antenna in 65 nm CMOS technology, in: Eur. Microw. Week 2014 Connect. Futur. EuMW 2014 - Conf. Proceedings; EuMC 2014 44th Eur. Microw. Conf., vol. 1, 2014, pp. 889–892.
[36] C. Hertleer, H. Rogier, L. Vallozzi, L. Van Langenhove, A textile antenna for off-body communication integrated into protective clothing for firefighters, IEEE Trans. Antennas Propag. 57 (4 PART. 1) (2009) 919–925.
[37] J.C. Wang, E.G. Lim, M. Leach, Z. Wang, K.L. Man, Review of wearable antennas for WBAN applications, IAENG Int. J. Comput. Sci. 43 (4) (2016) 474–480.

[38] A.Y.I. Ashyap et al, Robust and efficient integrated antenna with EBG-DGS enabled wide bandwidth for wearable medical device applications, IEEE Access 8 (2020) 56346–56358.
[39] T. Nakao, N.T. Hung, M. Nagatoshi, H. Morishita, Fundamental study on curved folded dipole antenna, in: IEEE Antennas Propag. Soc. AP-S Int. Symp., vol. 2, 2012, pp. 2–3,.
[40] P. Salonen, L. Sydanheimo, M. Keskilammi, M. Kivikoski, Small planar inverted-F antenna for wearable applications, in: Int. Symp. Wearable Comput. Dig. Pap., 1999, pp. 95–100.
[41] C. Hertleer, A. Tronquo, H. Rogier, L. Vallozzi, L. Van Langenhove, Aperture-coupled patch antenna for integration into wearable textile systems, IEEE Antennas Wirel. Propag. Lett. 6 (2007) 392–395.
[42] A. Arif, M. Zubair, M. Ali, M.U. Khan, M.Q. Mehmood, A Compact, Low-Profile Fractal Antenna for Wearable On-Body WBAN Applications, IEEE Antennas Wirel. Propag. Lett. 18 (5) (2019) 981–985.
[43] R.K. Singh, A. Michel, P. Nepa, A. Salvatore, M. Terraroli, P. Perego, Compact and Wearable Yagi-Like Textile Antennas for Near-Field UHF-RFID Readers, IEEE Trans. Antennas Propag. 69 (3) (2021) 1324–1333.
[44] C. Mohan, S.E. Florence, Miniaturised Triangular Microstrip Antenna with Metamaterial for Wireless Sensor Node Applications, IETE J. Res. (2019) 1–6.
[45] X.Q. Zhu, Y.X. Guo, W. Wu, A Compact Dual-Band Antenna for Wireless Body-Area Network Applications, IEEE Antennas Wirel. Propag. Lett. vol. 15, no. c (2016) 98–101.
[46] J.S. Roh, Y.S. Chi, J.H. Lee, Y. Tak, S. Nam, T.J. Kang, Embroidered wearable multiresonant folded dipole antenna for FM reception, IEEE Antennas Wirel. Propag. Lett. 9 (2010) 803–806.
[47] W. Hu et al, Compact Wideband Folded Dipole Antenna with Multi-Resonant Modes, IEEE Trans. Antennas Propag. 67 (11) (2019) 6789–6799.
[48] F.R. Hsiao, K.L. Wong, Omnidirectional planar folded dipole antenna, IEEE Trans. Antennas Propag. 52 (7) (2004) 1898–1902.
[49] D.M. Gvozdic et al, The folded dipole: a self-balancing antenna, Microwave Opt. Technol. Lett. 29 (3) (2001) 155–160.
[50] W. Lin, R.W. Ziolkowski, Electrically Small, Single-Substrate Huygens Dipole Rectenna for Ultracompact Wireless Power Transfer Applications, IEEE Trans. Antennas Propag. 69 (2) (2021) 1130–1134.
[51] M.M. Mostafa, T.M. Abuelfadl, A.M.E. Safwat, AMC loaded folded dipole with heart-shaped radiation pattern, Electron. Lett. 54 (18) (2018) 1061–1062.
[52] R. Gonçalves, N.B. Carvalho, P. Pinho, Small antenna design for very compact devices and wearables, IET Microwaves, Antennas Propag. 11 (6) (2017) 874–879.
[53] M. El Atrash, O.F. Abdalgalil, I.S. Mahmoud, M.A. Abdalla, S. R. Zahran, Wearable high gain low SAR antenna loaded with backed all-textile EBG for WBAN applications, IET Microwaves, Antennas Propag. 14 (8) (2020) 791–799.
[54] Y. Wu, J.P. Linnartz, Effects of Antenna Mutual Coupling on the Performance of MIMO Systems, in: 29th Symp. Inf. Theory Benelux, no. May, 2008, pp. 1–8.
[55] S.M. Saeed, C.A. Balanis, C.R. Birtcher, A Wearable and Reconfigurable Folded Slot Antenna for Body-Worn Devices, 2017 IEEE Antennas Propag. Soc. Int. Symp. Proc., vol. 2017-Janua, 2017, pp. 575–576.
[56] C. Balanis, Antenna Theory: Analysis and Design, 4th ed., Wiley, Hoboken, NJ, USA, 2016.
[57] S.A. Balakrishnan, E.F. Sundarsingh, Conformal self-balanced EBG integrated printed folded dipole antenna for wireless body area networks, IET Microwaves, Antennas Propag. 13 (14) (2019) 2480–2485.
[58] J. Joubert, J.C. Vardaxoglou, W.G. Whittow, J.W. Odendaal, CPW-fed cavity-backed slot radiator loaded with an AMC reflector, IEEE Trans. Antennas Propag. 60 (2 PART 2) (2012) 735–742.
[59] S. Yan, P.J. Soh, G.A.E. Vandenbosch, Low-profile dual-band textile antenna with artificial magnetic conductor plane, IEEE Trans. Antennas Propag. 62 (12) (2014) 6487–6490.
[60] S.X. Ta, I. Park, Dual-band low-profile crossed asymmetric dipole antenna on dual-band AMC surface, IEEE Antennas Wirel. Propag. Lett. 13 (2014) 587–590.